Magnetic Resonance in Medicine 56:481–488 (2006)

Targeted-HASTE Imaging With Automated Device Tracking for MR-Guided Needle Interventions in Closed-Bore MR Systems

H. Zimmermann,[1] S. Müller,[1] B. Gutmann,[2] H. Bardenheuer,[3] A. Melzer,[4] R. Umathum,[1] W. Nitz,[5] W. Semmler,[1] and M. Bock[1*]

Percutaneous MR-guided interventions with needles require fast pulse sequences to image the needle trajectory with minimal susceptibility artifacts. Spin-echo pulse sequences are well suited for reducing artifact size; however, even with single-shot turbo spin-echo techniques, such as rapid acquisition with relaxation enhancement (RARE) or half-Fourier acquisition single-shot turbo spin-echo (HASTE), fast imaging remains challenging. In this work we present a HASTE pulse sequence that is combined with inner-volume excitation to reduce the scan time and limit the imaging field of view (FOV) to a small strip close to the needle trajectory (targeted-HASTE). To compensate for signal saturation from fast repeated acquisitions, a magnetization restore pulse (driven equilibrium Fourier transform (DEFT)) is used. The sequence is combined with dedicated active marker coils to measure the position and orientation of the needle so that the targeted-HASTE image slice is automatically repositioned. In an animal experiment the coils were attached to an MR-compatible robotic assistance system for MR-guided interventions. Needle insertion and infusion via the needle could be visualized with a temporal resolution of 1 s, and the needle tip could be localized even in the presence of a stainless steel mandrel. Magn Reson Med 56:481–488, 2006. © 2006 Wiley-Liss, Inc.

Key words: fast MRI; percutaneous intervention; interventional devices; device localization; DEFT; inner volume imaging; local look (LoLo)

Currently, interventions with MR guidance are primarily performed in open MR systems, which provide better access to the patient. Unfortunately, open clinical systems with field strengths below 1 Tesla suffer from low signal-to-noise ratios (SNRs). Furthermore, gradient systems are limited in strength, slew rate, and homogeneity, which affects both image update rates and quality. The main advantage of high-field systems is that the higher SNR allows for faster signal sampling with image update rates of several images per second. For these reasons it is desirable to perform interventions in closed-bore, high-field MR systems.

During percutaneous interventions with needles, the closed-bore construction of high-field systems can be partially compensated for by passive or active robotic assistance systems that give mechanical stability to the needle trajectory (1). Commercial breast biopsy systems, for example, use dedicated breast coils with passive markers and grid systems to both hold and position the biopsy needle. Recently a fully MR-compatible robotic assistance system was developed (2) that consists of a pneumatically driven robot arm and a distal instrument holder. With this system the needle trajectory is defined using initial planning images of the target region. The assistance system then places the needle tip at the skin insertion point and aligns the instrument with the planned trajectory. Finally, the operator manually advances the needle to the target point.

During advancement of the needle, continuous image guidance can become necessary in anatomical regions where motion is present. For example, if the needle is inserted into a liver lesion, breathing motion will cause a cyclic displacement of tissue in the head–feet direction, which may lead to substantial differences between the planned and the actual needle trajectory. Unfortunately, optimized real-time pulse sequences for needle display, which are less susceptible to needle artifacts and automatically align the image slice with the current needle orientation to avoid time-consuming interaction with the MR scanner, are not clinically available (3).

Depending on the clinical application, MR-guided interventions require near real-time imaging with image update rates of 1 Hz or higher. Therefore, fast gradient-echo techniques such as fast low-angle shot (FLASH), fast imaging with steady precession (FISP), or balanced steady-state free precession (bSSFP, trueFISP) are used, which suffer from increased susceptibility artifacts as compared to the slower spin-echo techniques. With the advent of half-Fourier acquisition single-shot turbo spin-echo (HASTE) pulse sequences, many applications in abdominal imaging, such as the visualization of liquid-containing lesions, have become possible because they provide excellent T_2 contrast at subsecond imaging times. As demonstrated recently (4), a fast single-shot spin-echo technique with contrast enhancement can also be applied for repeated real-time imaging. This technique combines a local look (LoLo, or inner volume) preparation (5,6) with a T_2-weighted single spin-echo readout and a magnetization restoration (7,8).

[1]Department of Medical Physics in Radiology, German Cancer Research Center (DKFZ), Heidelberg, Germany.

[2]Innomedic GmbH, Herxheim, Germany.

[3]Department of Anesthesiology, University of Heidelberg, Heidelberg, Germany.

[4]Department of Physical Engineering, University of Applied Sciences, Gelsenkirchen, Germany.

[5]Siemens Medical Solutions, Erlangen, Germany.

Presented in part at the 13th Annual Meeting of ISMRM, Miami, FL, USA, 2005.

*Correspondence to: Michael Bock, Dr. Rer. Nat. Dipl. Phys., Dept. Medical Physics in Radiology (E020), German Cancer Research Center (DKFZ), Im Neuenheimer Feld 280, 69120 Heidelberg, Germany. E-mail: m.bock@dkfz.de

Received 27 September 2005; revised 20 April 2006; accepted 3 May 2006.
DOI 10.1002/mrm.20983
Published online 22 June 2006 in Wiley InterScience (www.interscience.wiley.com).

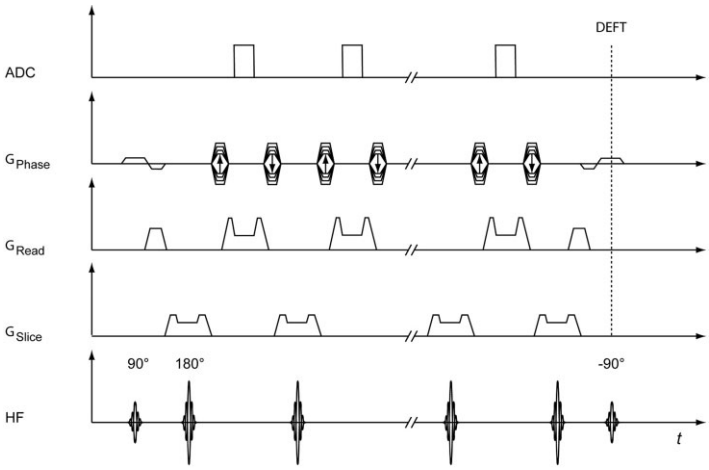

FIG. 1. Pulse sequence diagram of a targeted-HASTE sequence. A slice-selective 90° RF excitation is performed in the PE direction, and the slice thickness is given by the phase FOV. At the end of the echo train a DEFT pulse (i.e., a –90° RF pulse) is used to store the remaining transverse magnetization in the longitudinal direction.

The visualization and localization of devices in MR-guided interventions can be challenging because many instruments (e.g., needles) are visible only through their artifact. For localization and tracking of such instruments, different marker systems have been proposed, such as tuned fiducial markers (9), susceptibility markers (10), small receive coils (11), and optical systems (12,13) mounted onto the device. In the case of fiducial markers or small receive coils, the spatial localization can be realized within a few milliseconds using projection techniques (11).

In this work a fast HASTE pulse sequence was developed for percutaneous interventions. The pulse sequence was combined with automatic device tracking using position information from dedicated small marker receive coils to align the imaging slice with a needle. In combination with a robotic assistance system, the setup was evaluated in phantom and in vivo experiments.

MATERIALS AND METHODS

The experiments were performed on a clinical 1.5 T MR-scanner (Magnetom Symphony; Siemens, Erlangen, Germany) equipped with eight independent receiver channels and a 30 mT/m gradient system. The system has a magnet of 1.6 m length and 60 cm bore diameter, which is short enough so that an interventionalist standing at the magnet opening can manipulate devices at isocenter if they are reproducibly oriented and held in position by an external assistance system. A customized swivel-mounted MR-compatible monitor in the patient room was used to display the real-time images and to interact with the MR system software via a computer mouse. For MRI the standard spine-array coils were combined with a commercial flexible loop coil that was placed around the planned needle insertion point. In total, five of the eight receiver channels were reserved for imaging since three receive channels were occupied by the active markers.

Targeted-HASTE Pulse Sequence

For rapid acquisition of spin-echo images, a HASTE technique was used. As proposed in Ref. 4, this sequence was combined with a LoLo (5) or inner volume imaging (5) preparation whereby the initial 90° RF pulse is applied to a slice perpendicular to the subsequent 180° refocusing pulses (Fig. 1). Thus the signal is generated only in the overlap of the two slice volumes, which allows for an extreme reduction of the field of view (FOV) in the phase-encoding (PE) direction. The reduced number of PE steps shortens the echo train by a factor of 2 or more without any loss in spatial resolution.

As a consequence of the shorter echo train used, the spatial resolution in the PE direction is increased, particularly for tissues with short T_2. If the T_2 time is comparable to or shorter than the echo train, the image can be described by a convolution of the ideal *k*-space data with an exponential decay. This results in a non-ideal point spread function (PSF) with an associated loss of image detail (14) in small objects, which can be reduced by shortening the echo train length (ETL) using various techniques, such as parallel imaging (15). In Fig. 2 a conventional HASTE pulse sequence (image resolution = 0.78 × 0.78 mm^2, slice thickness = 7 mm, TE = 81 ms, bandwidth = 130 Hz/pixel) with an ETL of 1385 ms is compared with a targeted-HASTE acquisition (34% PE-FOV) with an ETL of 530 ms in a resolution phantom (T_2 = 220 ms).

In repetitive imaging the signal of tissues with long T_1 times does not recover fully within the short TRs required for real-time imaging. This saturation leads to significant reductions in the available SNR. In tissues with long T_2 times, transverse magnetization is still present at the end of the spin-echo train, and a magnetization restoration pulse (driven equilibrium Fourier transform (DEFT)) can be used to partially compensate for the saturation (7,16). Therefore, a spin-echo is formed at the center of the restore pulse, which flips the magnetization into the positive *z*-direction. In Fig. 3 the effect of a targeted-HASTE acquisition with and without DEFT restoration is demonstrated in a volunteer experiment. A sagittal targeted-HASTE acquisition was performed with the following imaging parameters: TR = 2000 ms, TE = 126 ms, TA/image = 361 ms, slice thickness = 5 mm, spatial resolution = 0.98 × 0.98 mm^2, PE-FOV = 34%.

Before the imaging section, four Hadamard-encoded (17) projections (total acquisition time = 24 ms) were intro-

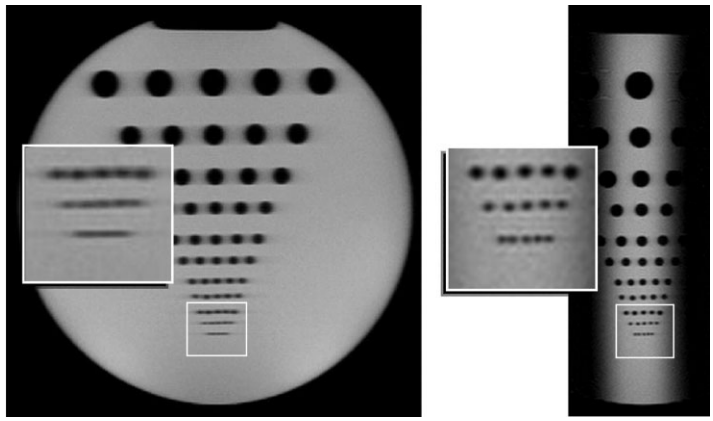

FIG. 2. Comparison of the spatial resolution of a conventional HASTE pulse sequence (left) and the corresponding targeted-HASTE image (right) of a resolution phantom. The targeted-HASTE image is sampled with a reduced number of *k*-space lines (34%), which results in a reduced blurring artifact in the PE direction (left–right). The smallest structures in the bottom row are about 1 mm in diameter.

duced to localize the small marker coils at the head of the assistance system. The spatial resolution of the projection measurements was fixed to 0.5 mm. A small excitation flip angle of 5°, which causes only a minimal perturbation of the magnetization, was used for the projection measurements. Using a custom-made image reconstruction program developed in the conventional reconstruction environment (Image Calculation Environment (ICE); Siemens, Erlangen, Germany), coil positions were calculated from the four projection measurements in less than 1 ms. At the gradient hardware controller the position information was used to define the slice position and orientation of the next targeted-HASTE image acquisition. Two different slice orientations with respect to the needle were implemented: in the standard orientation the slice was aligned with the needle, and in the perpendicular mode the slice orientation was orthogonal to the needle axis.

Active Marker Coils

Three small solenoid receive coils were constructed and used as active markers. The coils consisted of isolated copper wire (six turns, diameter = 5 mm) embedded in polymethylmethacrylate (PMMA, Plexiglas®) spheres that were filled with a 100:1 aqueous gadolinium-diethyltriaminepentaacetic acid (Gd-DTPA, Magnevist; Schering, Germany) solution (Fig. 4). The short T_1 of the liquid (about 50 ms) allows for fast magnetization recovery during the projection measurements for localization. Close to the coils, tuning and matching capacitors were integrated to match their impedance to 50 Ω. For signal reception each coil was connected to a separate receiver channel via an individual preamplifier. To avoid radiofrequency (RF) heating (18–20) by currents on the shield of the coaxial cable, multiple RF chokes (21) were incorporated.

Robotic Assistance System

To hold and position an instrument during a percutaneous intervention with both high mechanical stability and precision, the fully MR-compatible assistance system Innomotion (Innomedic, Herxheim, Germany) (2,22) was developed. The system consists of a robotic arm with six degrees of freedom, five of which are controlled remotely by pneumatic drives (Fig. 5). The arm is attached to a fiberglass arch that is mounted on the MR patient table. Through manual rotation the arm can be rotated on the arch by ±60° in steps of 30°. Initially, the coordinate systems of the MR scanner and assistance system are matched using the MR scanner's laser positioning system. At the distal end of the robotic arm an exchangeable application module is attached. Here the module consisted of a holder for coaxial needles. Additionally, four spheres filled with the same contrast agent solution were attached to the distal end. The passive markers are used by the software of the assistance system to finally align the gradient coordinate system of the MR with the robot's internal coordinate system. MR images of the passive markers are

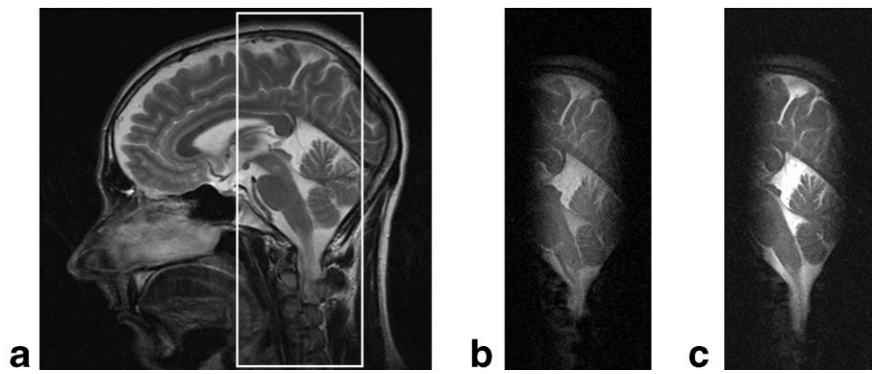

FIG. 3. Sagittal targeted-HASTE acquisition without (**b**) and with (**c**) DEFT magnetization restoration positioned in the brain of a volunteer (**a**). With the DEFT preparation the highest signal increase of about 35% is observed in the CSF-filled spaces.

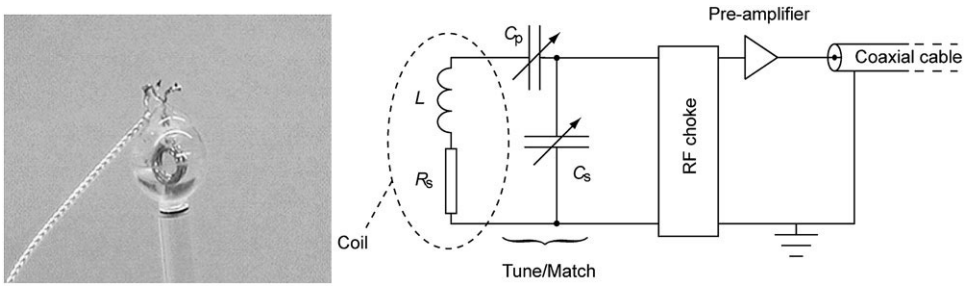

FIG. 4. **a:** The marker coil is embedded in a PMMA-sphere filled with 1:100 Gd-DTPA/H_2O solution. **b:** Equivalent circuit diagram of a marker coil: small serial (C_s) and parallel (C_p) capacitors were used to transform the coil's impedance (inductivity L, ohmic loss R_s) and to 50 Ω cable impedance.

acquired and sent as Digital Image Communication in Medicine (DICOM) data to the control computer of the assistance system, where their position is automatically detected and compared with the expected position using the internal optical position sensors. In addition to the passive markers, the three active marker coils were placed at the application module for automatic device tracking.

Phantom Experiments

To evaluate the accuracy of the marker localization, a marker coil was placed at different positions in the MR scanner. The results of the projection measurements were compared to the positions measured with a caliper gauge. The marker was moved along the *z*-axis at ($x = y = 0$ cm) and ($x = -15.6$ cm and $y = 0$ cm) between $z = -15$ cm and +15 cm (Fig. 6). To assess the signal quality of the projections, projection data were stored separately and the SNR was determined as the ratio of the peak signal intensity over the mean of the adjacent noise.

In a gelatin phantom containing small structures (grapes and tomatoes), we assessed in nine experiments whether the automatic slice positioning was able to align the targeted-HASTE image with the current needle position after the assistance system moved to the target position. In Fig. 7 a phantom measurement is shown in which a trajectory was planned at an angle of 22° so that the needle passed between an embedded grape and a tomato. After the robot arm was oriented, the targeted-HASTE pulse sequence was started with an arbitrary orientation and position of the imaging slice, and the final slice orientation angle after automatic slice definition was measured. During needle insertion, targeted-HASTE images were continuously acquired with a TR of 1 s (Fig. 7b and c) using the following parameters: TE = 35 ms, slice thickness = 5 mm, spatial resolution = 1.17 × 1.17 mm^2, PE-FOV = 41%, DEFT preparation. Finally, the needle placement was verified using a T_1-weighted multislice data acquisition (TR = 150 ms, TE = 2.1 ms, α = 60°, matrix = 256^2, FOV = 300 mm; Fig. 7a) and the needle artifact size was compared with a trueFISP image (TR = 4.4 ms, TE = 2.2 ms, α = 70°, matrix = 256^2, FOV = 300 mm). The orientation and center line of the targeted-HASTE imaging strip were compared with the planned needle angulation and the planned position of the insertion point.

Animal Experiment

In a female domestic pig (21 kg, 7 weeks old) a robot-assisted percutaneous needle insertion was performed in a manner similar to a therapeutic injection for the treatment of chronic pain. The animal experiment was approved by the Regierungspräsidium Karlsruhe (no. 35-9185.81/G-78/04). The sedated animal was placed on the MR table in a prone position. For initial sedation the animal received an intramuscular injection of 15 mg/kg body weight azaperon

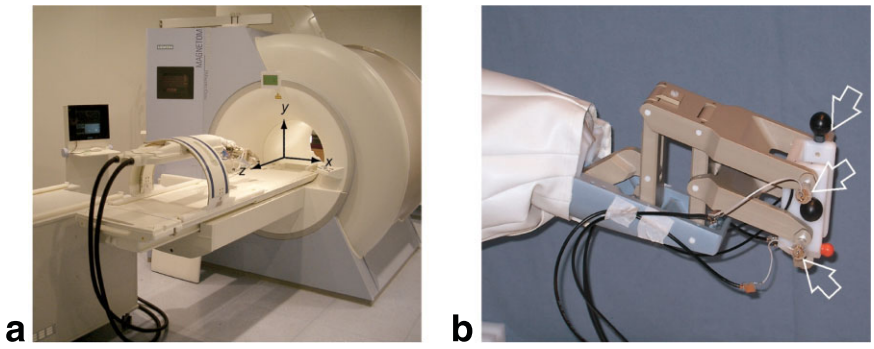

FIG. 5. **a:** Fully MR-compatible robotic assistance system for percutaneous interventions mounted on the patient table of a 1.5 T closed-bore MR system. The robotic arm can be manually rotated by ±60° on a fiberglass arc (1° of freedom). Arm motion in the other 5 degrees of freedom is controlled by fully MR-compatible pneumatic drives. The robotic assistance system is coregistered with the MR laser reference so that in subsequent MRI experiments identical coordinate systems can be used for robotic motion and MRI. **b:** At the distal end of the arm a needle holder with passive markers (black spheres) and three active marker coils (open arrows) is attached.

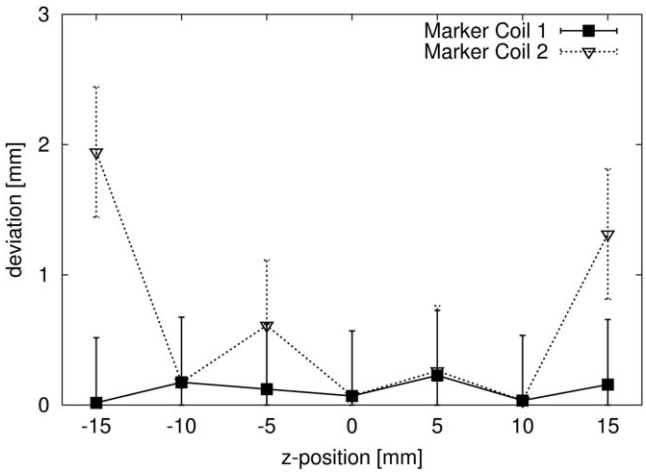

FIG. 6. Localization accuracy of a marker coil measurement along the z-axis. The deviation from the actual position was determined for different *z*-positions. Coil 1 was located in the magnet's isocenter at (*x, y*) = (0 cm, 0 cm) and coil 2 was at (–15.6 cm, 0 cm). The error bars indicate the precision of the projection measurement of 2 pixels, which corresponds to 1-mm spatial resolution.

(Stresnil; Janssen Pharmaceutica, Beerse, Belgium), 1 mg/kg body weight midazolam (Dormicum; Roche, Vienna, Austria), and 25 mg/kg body weight ketamine (Ketanest; Parke-Davis GmbH, Freiburg, Germany) and was then intubated and mechanically ventilated with halothane in a mixture of nitrous oxide and oxygen. Localizer images were acquired of the target region around the lumbar back musculature (m. erector spinae) at the level of the kidneys using T_1-weighted gradient-echo and balanced SSFP (trueFISP) pulse sequences (Fig. 8a). On a transverse slice an angulated needle trajectory was planned through the muscle pointing at the plexus coeliacus. Subsequently the assistance system automatically moved the needle to the insertion point.

Before manual needle insertion the targeted-HASTE image acquisition with automatic slice positioning was activated with the following parameters: TE = 34 ms, slice thickness = 7 mm, spatial resolution = 1.17 × 1.17 mm^2, PE-FOV = 38%, and DEFT preparation. Three different TR values (250 ms, 500 ms, and 1000 ms) were used to determine the SNR of muscle tissue. During the subsequent needle placement a TR of 1000 ms was chosen as a compromise between acquisition speed and SNR.

The interventionalist leaned into the magnet from the rear to introduce a 20 G low-artifact titanium coaxial puncture needle (Daum, Schwerin, Germany) with a maximum insertion length of 100 mm into the application module. The needle contained a stainless steel mandrel and was advanced slowly through the muscle until a resistance at the thoracolumbar fascia was noticed. Real-time targeted-HASTE images were continuously displayed to the interventionalist on the in-room monitor. After the mandrel was removed, an NaCl/Gd-DTPA solution (volume ratio: 5/1, volume: 10 ml) was infused through the needle and the distribution of the infusate was observed. In the targeted-HASTE images the contrast-to-noise ratio (CNR) was measured between the infused area and surrounding muscle tissue.

RESULTS

As shown in Fig. 2, the targeted-HASTE pulse sequence increased the observable spatial resolution over a conventional HASTE sequence with a full echo train. For the resolution phantom with a T_2 of 220 ms, a simulation resulted in a full width at half maximum (FWHM) for the PSF of about 3.2 mm and 1.4 mm, respectively. The increased spatial resolution is clearly visualized in the bottom row of the phantom, where 1-mm Plexiglas rods are embedded. The inclusion of the DEFT preparation provided a signal gain of about 35% in the cerebrospinal fluid (CSF), as shown in the volunteer experiment in Fig. 3, whereas for gray or white matter the intensity did not change.

The results of the localization experiments with the marker coils are presented in Fig. 6. The measured SNR of the marker coil signal in the projections was found to be in the range of 100–1000, and thus an unambiguous identification of the coil signal was always possible. For the coil at $x = y = 0$ cm the maximum deviation was less than

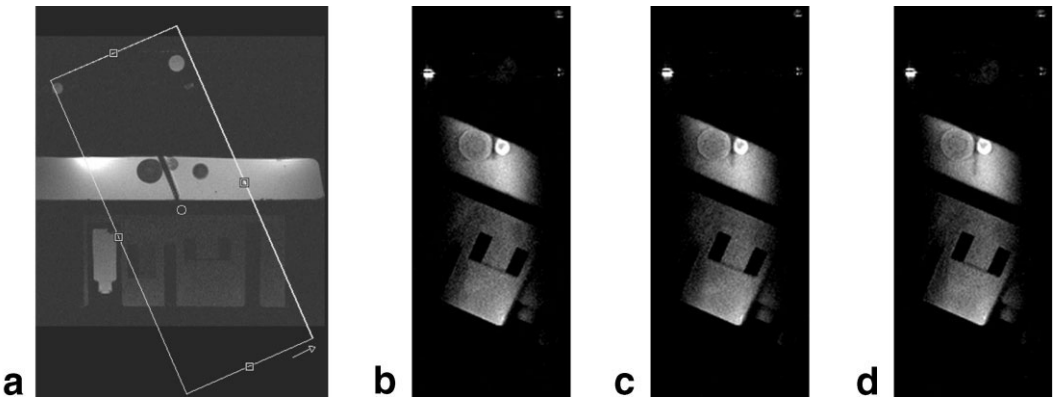

FIG. 7. **a:** Verification of the needle placement in a gel phantom. The artifact of a 20 G needle with a titan mandrel is significantly larger (Ø ≈ 4 mm) than the needle itself. In the subsequent real-time targeted-HASTE images (**b–d**) the needle motion is visualized at an update rate of 1 Hz in an image orientation that is automatically aligned parallel to the needle trajectory.

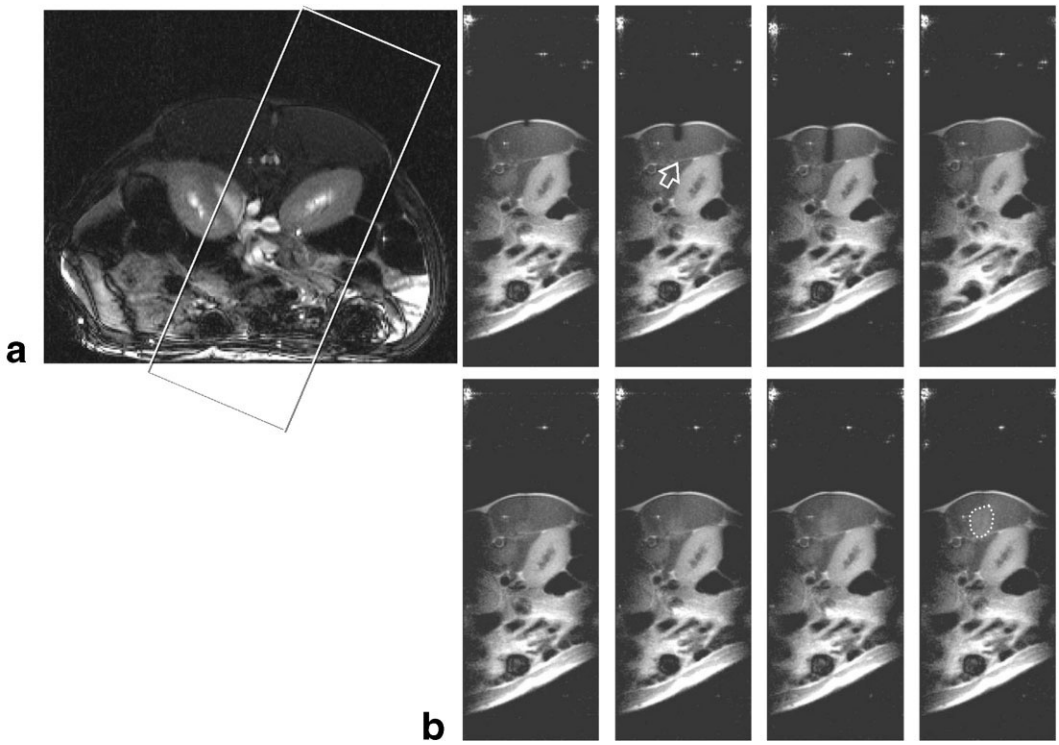

FIG. 8. **a:** On the trueFISP localizer an angulated needle trajectory was planned. **b:** The first three targeted-HASTE time frames show the insertion of the needle with a stainless steel mandrel until the tip reaches the thoracolumbar fascia (open arrow). Note that the PE direction is from left to right. In the fourth image the mandrel is removed and only a faint needle artifact remains. The last four time frames show the slow infusion of the contrast agent solution. The solution is visible as a hyperintense area (dotted line) that is expanding backwards along the needle trajectory.

0.5 mm for all measured z-positions, whereas the deviation was found to increase substantially to about 2 mm at $z = \pm 15$ cm for the off-center coil measurements.

The nine experiments in the gel phantom showed that the targeted-HASTE sequence could automatically adjust the position and orientation of the imaging slice with the needle trajectory (Fig. 7). In all experiments the deviation between the planned needle angulation and targeted-HASTE slice rotation was less than 1°, and the insertion point was localized in the center of the imaging strip with a precision of 1.2 mm. The thickness of the needle artifact with the stainless steel mandrel was about 8 mm, which is substantially smaller compared to that in a conventional trueFISP acquisition (≈18 mm). During the needle insertion the targeted-HASTE images were displayed with no noticeable latency. The images proved to be helpful for the fine adjustment of the needle trajectory, which was achieved by applying slight lateral pressure to the needle shaft. Because of the active position stabilization of the assistance system, the slice position measured by the marker coils did not change when the pressure was applied.

In the animal experiments, SNRs in muscle tissue of about 5.6, 1.7, and 1 were found for TR values of 1000 ms, 500 ms, and 250 ms, respectively. The longest TR value was chosen for the subsequent real-time imaging to visualize the needle with an optimal contrast while maintaining an acceptable temporal resolution. During needle insertion the instrument trajectory was visualized with high contrast (Fig. 8). Taking into account the needle artifact, the tip of the needle was well visualized, as can be seen in the time frame, where the needle approaches the thoracolumbar fascia. The needle artifact is caused mainly by the stainless steel mandrel, since the needle itself is hardly visible in the targeted-HASTE images after the mandrel is removed. The contrast agent infusion could be clearly visualized with the targeted-HASTE sequence at a CNR of $(377 - 261)/20 = 5.8$ (mean signal intensity in target region minus mean signal of surrounding muscle tissue over the standard deviation in an artifact-free background region).

DISCUSSION

In this work a real-time HASTE sequence was combined with active coil tracking and LoLo preparation to follow the pathway of a needle during an MR-guided intervention. The implemented targeted-HASTE sequence was evaluated using an MR-compatible robotic assistance system.

As expected, the LoLo technique increased the observable spatial resolution in tissues in which the T_2 relaxation time is on the order of the ETL. Typically, a PE reduction factor of 30–40% is used in the targeted-HASTE sequence, which leads to a theoretical reduction of the SNR over a full k-space acquisition of 0.55–0.63, since SNR is proportional to the square root of the number of k-space lines. However, the predominant signal loss in the targeted-HASTE sequence is caused by signal saturation from the

repetitive measurements. This saturation is partially compensated for by the DEFT magnetization restoration. Nevertheless, TRs on the order of 1 s were necessary to visualize the needle in muscle tissue with sufficient contrast. The SNR could be increased by using lower readout bandwidths; however, this would also increase the ETL, which would decrease the time available for T_1 relaxation after the end of the echo train.

The automatic slice positioning was found to be very helpful during the intervention, since no additional interaction between the interventionist and MR user interface was necessary. Using conventional fast gradient-echo techniques such as FLASH or trueFISP, the time required to localize the imaging plane after the assistance system has reached its position can easily amount to 1 min or more (in this study automatic slice positioning was able to find the needle position in about 1 s). Furthermore, automatic slice adjustment could be useful in situations in which the needle is moving, such as in anatomical regions where breathing motion is present. However, this would require a tight coupling between the marker coils and needle.

The accuracy of the coil detection was very high near isocenter, but decreased with increasing distance. This was as expected, since no corrections for gradient inhomogeneities were performed. In the experiments the three marker coils were attached to the instrument head and positioned at a maximum distance of 10 cm. Gradient imperfections can be characterized and corrected by a polynomial expansion of the actual gradient field (23–25). Near the isocenter, where local changes in the field are typically small, all marker coil positions are shifted predominantly in the same direction. This affects the imaging slice offset, but has only a minor effect on the slice orientation. At a slice thickness of 7 mm the slice shift is still acceptable, since the needle remains in the imaging slice. Nevertheless, in future refinements of the algorithm a distortion correction of the coil coordinates will be applied.

A major advantage of the targeted-HASTE pulse sequence is its insensitivity to susceptibility artifacts. Even in the presence of a stainless steel mandrel the tip of the needle could be visualized, and the needle outline was seen with nearly no artifact after the mandrel was removed. This indicates that the targeted-HASTE technique offers the possibility of performing MR-guided interventions with an instrumentation that does not necessarily have to consist of dedicated materials, such as Nitinol. In this experiment the MR-compatible needle itself was hardly visible at the chosen spatial resolution. Since the needle artifact, and thus the needle conspicuity, can be increased by lowering the readout bandwidth, it should also be possible to perform targeted-HASTE imaging with MR-compatible instruments.

The LoLo technique used for the targeted-HASTE sequence has the disadvantage that a simultaneous image acquisition in a slice parallel to the needle plane is not possible, since the 90° preparation in the orthogonal slice already saturates the MR signal. For an MR-guided intervention with needles, additional parallel slices would be desirable to detect needle deflections or needle bending, which cannot be measured by the marker coils at the needle holder. A possible solution to this problem would be to acquire adjacent slices in subsequent TR intervals; however, this would reduce the temporal resolution even further. Another approach is to use nonorthogonal 90° and 180° slices, which have been proposed for diffusion imaging (26). In this approach a shallow angle between the 90° and 180° slice, and the desired slice plane is chosen such that areas in parallel imaging planes are not subjected to RF excitations. The applicability of this technique to interventional studies remains to be investigated.

In the animal experiment the temporal resolution of 1 s was sufficient to safely advance the needle in the MR magnet. Gradient-echo imaging techniques, such as FLASH and trueFISP, provide higher image frame rates at comparable spatial resolution; however, the artifact size in these images is much greater, which makes it more difficult to advance the needle precisely to smaller targets, such as nerve roots. The diffusion of the injected contrast agent solution could be visualized with the targeted-HASTE sequence. An improved contrast between muscle and contrast agent could have been achieved with an optimized T_1-weighted sequence, but a change of sequence would have prolonged the total procedure time. To increase the T_1 contrast during contrast agent infusion, it would be possible to shorten the TR of the targeted-HASTE sequence at run time through a dedicated real-time interface (27).

Recently a steady-state version of the LoLo technique, termed selective missing pulse SSFP (MP-SSFP) (28), was proposed. This technique can be applied without additional time delays between the acquisition of two images. Unfortunately, this pulse sequence uses relatively long TRs of 27 ms and low receiver bandwidths. For a typical value of 40 PE steps, this would also result in a temporal resolution of 1 s, which is comparable to the time resolution of the targeted-HASTE sequence. Furthermore, low receiver bandwidths would introduce significant susceptibility artifacts that are avoided by the targeted-HASTE technique.

In the current experiments a robotic assistance system was used to hold, orient, and stabilize the puncture needle. In principle, a less technically demanding approach using a small hand-held needle tracking system, in which the tracking coils are attached to the needle shaft (29), could be used. Unfortunately, it can be challenging to stabilize such a needle holder in closed-bore MRI systems because the radiologist has to simultaneously view the real-time images on the in-room monitor and manipulate the needle holder close to magnet isocenter. Additionally, it is difficult to plan the needle trajectory prior to insertion.

The presented pulse sequence offers the possibility of monitoring an MR-guided intervention with a typical frame rate of 1 Hz and a spatial in-plane resolution of about 1 mm. In combination with a robotic assistance system for needle guidance and automatic slice positioning, the sequence was evaluated in phantom and animal experiments. For many interventional procedures, such as MR-guided biopsies, therapeutic injections for pain, drainage, or local tumor therapy, this technique could be applied to accelerate the intervention. Furthermore, continuous image control is expected to reduce the number of failures, since risk organs along the trajectory can be actively avoided and it should be possible to achieve better control over the therapeutic distribution volume.

ACKNOWLEDGMENTS

The authors thank Barbara Dillenberger, Roland Galmbacher, and Hamid Ghaderi for their support during the animal experiments, and Thomas Remmele, Stefanie Guthmann, and Andreas Berger from Innomedic for their help with the assistance system.

REFERENCES

1. Felden A, Vagner J, Hinz A, Fischer H, Pfleiderer SO, Reichenbach JR, Kaiser WA. ROBITOM-robot for biopsy and therapy of the mamma. Biomed Tech (Berl) 2002;47(Suppl 1 Pt 1):2–5.
2. Gutmann B, Lukoschek A, Fischer H, Bock M, Melzer A. Development of an assistant robotic system for interventional radiology inside CT and MR scanners. In: 2. Jahrestagung der Deutschen Gesellschaft für Computer-und Roboterassistierte Chirurgie (CURAC), Nümberg, Germany, 2003. p C-II-6.
3. Bock M, Volz S, Zühlsdorff S, Umathum R, Fink C, Hallscheidt P, Semmler W. MR coil design for simultaneous tip tracking and curvature delineation of a catheter. Magn Reson Med 2004;52:214–218.
4. Makki M, Graves MJ, Lomas DJ. Interactive body magnetic resonance fluoroscopy using modified single-shot half-Fourier rapid acquisition with relaxation enhancement (RARE) with multiparameter control. J Magn Reson Imaging 2002;16:85–93.
5. Feinberg DA, Hoenninger JC, Crooks LE, Kaufmann L, Watts JC, Arakawa M. Inner volume MRI: technical concepts and their application. Radiology 1985;156:743–747.
6. Buecker A, Adam G, Neuerburg JM, Glowinski A, Vaals van JJ, Guenther RW. MR-guided biopsy using a T_2-weighted single-shot zoom imaging sequence (local look technique). J Magn Reson Imaging 1998; 8:955–959.
7. Becker ED, Ferretti JA. Driven equilibrium Fourier transform spectroscopy. J Am Chem Soc 1969;91:7784–7785.
8. Maki JH, Johnson GA, Cofer GP, MacFall JR. SNR improvement in NMR microscopy using DEFT. J Magn Reson 1988;80:482–492.
9. Burl M, Coutts GA, Young IR. Tuned fiducial markers to identify body locations with minimal perturbation of tissue magnetization. Magn Reson Med 1996;36:491–493.
10. Bakker CJ, Hoogeveen RM, Hurtak WF, van Vaals JJ, Viergever MA, Mali WP. MR-guided endovascular interventions: susceptibility-based catheter and near-real-time imaging technique. Radiology 1997;202: 273–276.
11. Ackerman JL, Offut MC, Buxton RB, Brady TJ. Rapid 3D tracking of small RF coils. In: Proceedings of the 5th Annual Meeting of SMRM, Montreal, Canada, 1986. p 1131.
12. Silverman SG, Collick BD, Figueira MR, Khorasani R, Adams DF, Newman RW, Topulos GP, Jolesz FA. Interactive MR-guided biopsy in an open-configuration MR imaging system. Radiology 1995;197:175–181.
13. Ojala R, Sequeiros RB, Klemola R, Vahala E, Jyrkinen L, Tervonen O. MR-guided bone biopsy: preliminary report of a new guiding method. J Magn Reson Imaging 2002;15:82–86.
14. Constable RT, Gore JC. The loss of small objects in variable TE imaging: implications for FSE, RARE, and EPI. Magn Reson Med 1992;28:9–24.
15. Griswold MA, Jakob PM, Chen Q, Goldfarb JW, Manning WJ, Edelman RR, Sodickson DK. Resolution enhancement in single-shot imaging using simultaneous acquisition of spatial harmonics (SMASH). Magn Reson Med 1999;41:1236–1245.
16. Busse RF, Riederer SJ, Fletcher JF, Bharucha AE, Brandt KR. Interactive fast spin-echo imaging. Magn Reson Med 2000;44:339–348.
17. Dumoulin CL, Souza SP, Darrow RD. Real-time position monitoring of invasive devices using magnetic resonance. Magn Reson Med 1993;29: 411–415.
18. Nitz WR, Oppelt A, Renz W, Manke C, Lenhart M, Link J. On the heating of linear conductive structures as guide wires and catheters in interventional MRI. J Magn Reson Imaging 2001;13:105–114.
19. Ladd ME, Quick HH. Reduction of resonant RF heating in intravascular catheters using coaxial chokes. Magn Reson Med 2000;43:615–619.
20. Yeung CJ, Susil RC, Atalar E. RF heating due to conductive wires during MRI depends on the phase distribution of the transmit field. Magn Reson Med 2002;48:1096–1098.
21. Tischer F. Anordnung zur Unterdrückung des auf die Außenseite des Mantels einer konzentrischen Ultrakurzwellenleitung an einer Unterbrechungsstelle übertretenden Hochfrequenzstomes. German patent no. 733 697; 1939.
22. Melzer A, Gutmann B, Lukoschek A, Mark M, Zylka W, Fischer H. Experimental evaluation of an MR compatible telerobotic system for CT/MR-guided interventions. Radiol Suppl 2003;44:409.
23. Sekihara K, Kuroda M, Kohno H. Image restoration from non-uniform magnetic field influence for direct Fourier NMR imaging. Phys Med Biol 1984;29:13–24.
24. Roméo F, Hoult DI. Magnet field profiling: analysis and correcting coil design. Magn Reson Med 1984;1:44–65.
25. Bernstein MA, Xiaohong JZ, Polzin JA, King KF, Ganin A, Pelc NJ, Glover GH. Concomitant gradient terms in phase contrast MR: analysis and correction. Magn Reson Med 1998;39:300–308.
26. Maier SE. Slab scan diffusion imaging. Magn Reson Med 2001;46: 1136–1143.
27. Volz S, Zuehlsdorff S, Thesen S, Meyer H, Nitz W, Umathum R, Semmler W, Bock M. Automatic and interactive device tracking in interventional MR. Eur Radiol 2002;12:F29.
28. Hwang KP, Flask C, Lewin JS, Duerk JL. Selective missing pulse steady state free precession (MP-SSFP): inner volume and chemical shift selective imaging in a steady state sequence. J Magn Reson Imaging 2004;19:124–132.
29. Zimmermann H, Zuehlsdorff S, Volz R, Umathum R, Semmler W, Bock M. Local-look HASTE MRI with interactive slice positioning for an active needle system. In: Proceedings of the 12th Annual Meeting of ISMRM, Kyoto, Japan, 2004. p 955.